Supplementary Material

Absolute film separation of dyes/salts and emulsions with a superhigh water permeance through graded nanofluidic channels

Tianmeng Zhang[a], Ruyong Guo[a], Guobing Ying[a], Zhiyong Lu[a], Chao Peng[b], Mingxia Shen[a], Jianfeng Zhang*[a]

[a]College of Mechanics and Materials, Hohai University, Nanjing 211100, PR China

[b]Productivity Centre of Jiangsu Province, Nanjing 210042, China

* Corresponding author, Email address: jfzhang_sic@163.com

Theories

Principles of numerical simulation of particle accumulation

Solids with a large number of pores formed by the accumulation of spherical particles belong to the porous media of particle accumulation. Model simulations of fluid percolation and circulation between granular media are considered to solve the continuous and N-S equations in the Euler-Cartesian coordinate system[1]. The continuity equation and the N-S equation for a fluid in a fluid-solid two-phase medium are as follows:

$$\frac{\partial n}{\partial t} = -(\nabla nu)$$

$$\frac{\partial (nu)}{\partial t} = -(\nabla nuu) - \frac{n}{\rho \mathrm{f}}\nabla p - \frac{n}{\rho \mathrm{f}}\nabla \tau + ng + \frac{f\mathrm{int}}{\rho \mathrm{f}}$$

where $\boldsymbol{u}$ is the flow velocity vector, $\boldsymbol{t}$ is the viscous stress tensor, $\boldsymbol{g}$ is the acceleration of gravity and $\boldsymbol{f}_{\mathbf{int}}$ is the interaction force between the particles and the fluid per unit volume.

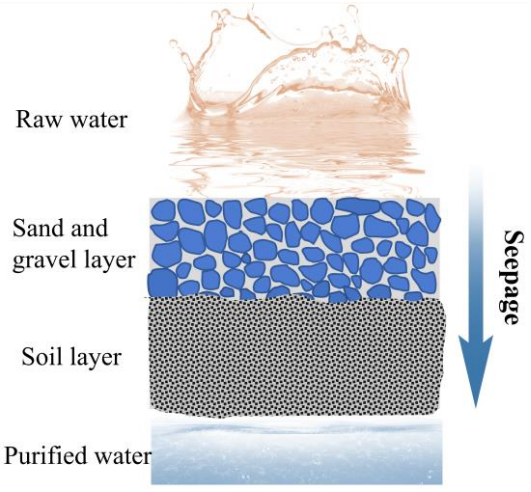

Fig. S1. The process of water purification by sandy soil layer

The percolation of water in sandy soils, for example, can be approximated as the flow of a fluid through a granular accumulation medium. Related research dates back to 1856 when Darcy experimentally concluded that the pressure gradient was proportional to the flow rate:

$$\frac{\mathrm{d}p}{\mathrm{d}x} = -\frac{\upsilon \mathrm{f} \rho \mathrm{f}}{k} ux0$$

The equation can better simulate the actual granular layer after continuous improvement and correction：

$$\frac{\mathrm{d}p}{\mathrm{d}x} = -(150\frac{(1-n)^2}{n^3 \bar{d}^{-2}\mathrm{p}} \upsilon \mathrm{f}\, \rho \mathrm{f}\, ux0 + 1.75\frac{(1-n)\rho \mathrm{f}}{n^3 \bar{d}\mathrm{p}} ux0^2)c$$

where $\boldsymbol{\rho_f}$ and $\boldsymbol{\upsilon_f}$ are the density and viscosity coefficient of the fluid, $\boldsymbol{u_{x0}}$ is the mean flow velocity and $\boldsymbol{k}$ is the permeability coefficient.

Film surface fluid flow model

In order to gain a clearer understanding of the mechanisms inherent in the filtration of aqueous solutions by films, researchers have used mathematical concepts to generalize the filtration process into mathematical models with generally applicable laws. The controlling equation for fluid flow at the film surface is as follows:

$$\nabla \cdot \bar{U} = 0$$

$$\frac{\partial \bar{U}}{\partial t} + (U \cdot \nabla)\bar{U} = -\frac{1}{\rho}\nabla P + \mu \nabla^2 \bar{U} c$$

where $\bar{\boldsymbol{U}}$ is the velocity vector of the fluid, $\boldsymbol{\mu}$ is the dynamic viscosity coefficient, $\boldsymbol{\rho}$ is the fluid density and $\boldsymbol{\nabla p}$ is the pressure gradient.

Mechanism of film permeance change

In the film separation process, the presence of film contamination problems can lead to permeate flux degradation and low separation efficiency over time. Types of film contamination include: intra-pore adsorption, pore plugging by macromolecules or particles, surface adsorption, formation of a cake layer. For pressure-driven film separation processes, the permeate flux of the film can be expressed as:

$$J = \frac{1}{A} \cdot \frac{dVP}{dt} = \frac{\Delta p}{\mu RTotal}$$

$$RTotal = Rm + Rcp + Rc + Rp$$

Where $\boldsymbol{J}$ is the permeate flux, $\boldsymbol{A}$ is the permeate area, $\boldsymbol{V_p}$ is the total permeate volume, $\boldsymbol{t}$ is the filtration time, $\boldsymbol{\Delta p}$ is the transfilm pressure, $\boldsymbol{\mu}$ is the permeate viscosity, $\boldsymbol{R_m}$ is the film's own resistance, $\boldsymbol{R_{cp}}$ is the concentration polarization resistance, $\boldsymbol{R_c}$ is the cake layer resistance, and $\boldsymbol{R_p}$ is the pore plugging resistance.

Materials

Pyrrole (Py), urea (≥ 99.0 %) and hydrogen peroxide (H_2O_2, 30%) were obtained

from Aladdin Chemical Reagent Co., Ltd. (Shanghai, China). Bacterial cellulose was purchased from Guilin Qihong Technology Co., Ltd. (Guangxi, China). The dyes involved in the experiments were purchased from China Pharmaceutical Group Co., Ltd. (Shanghai, China). Tween 80 was purchased from J&K Scientific Co. Ltd.

Experimental procedure

Synthesis of PPSM and PBC

Firstly, 0.1 g of $FeCl_2 \cdot 4H_2O$ was dissolved in 60mL of distilled water, and then 1ml of pre-dispersed pyrrole monomer was added and stirred for 30 minutes. Then 5 mL of H_2O_2 (30 wt%) was added and stirred at room temperature for 12 h. The precipitate was collected by centrifugation and washed several times with acetone and deionized water. Finally, polypyrrole sub-micron spheres, abbreviated as PSM, were obtained by drying at 60 °C. 0.1g of PSM was dispersed in Tris-HCl solution (pH=8.5), then 0.1g of dopamine hydrochloride was added and the reaction was stirred for 10h. The final reaction product was washed by centrifugation and dried under vacuum to obtain PDA-coated polypyrrole sub-micron spheres, which were abbreviated as PPSM.

PPy was modified on the BC through chemical oxidation polymerization. First, 2.1 mL of pyrrole monomer was dispersed in 6 mL of ethanol, then added to 50 mL of BC dispersion (1.5 mg/mL) and stirred in an ice bath for 1 h. Then 50 mL of HCl solution (2M, and 0.84g of $FeCl_3 \cdot H_2O$) was added dropwise and stirred for 10 h. The product PBC was obtained by filtering and washing to remove unreacted monomer and impurities. Finally, the product was dispersed in 200 mL of aqueous solution (sodium dodecyl benzene sulfonate: 1 mg/mL) to obtain PBC dispersion of about 3 mg/mL.

Preparation of PBC/PPSM composite film

The PBC/PPSM composite films were prepared by the process of vacuum-assisted filtration. A certain amount of pre-prepared PBC dispersion was vacuum filtered onto the commercial hybrid film. Next, the ultrasonically dispersed homogeneous PPSM dispersion is filtered onto the PBC film. The PBC/PPSM composite films was obtained and marked with PBC/PPSM. According to the pure water permeance of the composite film obtained from different loading amounts of PBC and PPSM (Fig. S10, Supporting Information), the PBC/PPSM composite film was selected with a loading amount of 33.3 g m^{-2} for PBC and 8.25 g m^{-2} for PPSM. Similarly, the PBC/PSM composite film was fabricated according to the same steps and loading amount as above.

Characterization of dye rejection and salt permeation

Dye rejections of as-obtained film were investigated using a dead-end and cross-flow filtration device. It is worth noting that concentration polarization may occur during the separation of dyes by dead-end filtration. All films need to be filtered through pure water before being tested until the permeance is stable. The water permeance was recorded by measuring the amount of water collected at a

transfilm pressure of 0.4-1 bar (Dead-end filter pressure of 1 bar; Cross-flow filter pressure of 0.4 bar). The retention performance of the film was assessed by the concentration of the solution before and after filtration tested by UV/vis spectrophotometer. Simulation of high-salt wastewater and high-salt organic wastewater tests by configuring different concentrations (1 %, 3 %, 5 %) of salt solutions. The common types of ions in high-salt organic wastewater are replaced by three salts (NaCl, Na_2SO_4, $CaCl_2$). The concentration of salt in the solution was measured by testing the conductivity of the solution.

The permeance J (L m^{-2} h^{-1} bar^{-1}) and rejection R (%) were calculated by the following equation 1 and 2, respectively:

$$J = \frac{V}{A\,\Delta t\,\Delta P} \quad (1)$$

$$R = \left(1 - \frac{C}{C_0}\right) \times 100\% \quad (2)$$

where V (L) was the volume of permeated water, A (m^2) was the effective film area, Δt (h) was the operation time, ΔP (bar) is the transfilm pressure, and C and C_0 are the dye or salt concentrations of the filtrate and initial solution, respectively.

Characterization of oil-in-water emulsion separation

Different types of oil-in-water (O/W) emulsions were used to evaluate the separation properties of the films. Emulsion formulation: 2ml of oil (vacuum pump oil, hexadecane, liquid paraffin, polydimethylsiloxane) and 0.2 g of Tween 80 were added to 98ml of pure water and stirred continuously for 8h to obtain the vacuum pump oil-in-water (V/W) emulsion, hexadecane-in-water (H/W) emulsion, liquid paraffin-in-water (L/W) emulsion, polydimethylsiloxane-in-water (P/W) emulsion, respectively. As with dye filtration, dead-end filtration was also used in oil-water separation tests, and the water permeance and rejection rate are calculated using equations 1, 2.

Microstructural characterization

The scanning electron microscope (SEM, FEI Inspect F50, USA) and transmission electron microscopy (TEM, JEM-2100, JEOL, Japan) were used to observe the micro-morphologies of raw materials and films. The roughness of these films was tested on an atomic force microscopy (AFM, Bruker Dimension ICON). The wettability of each film was got from the contact angle measuring instrument (WCA, Data physics) at room temperature. X-ray diffraction (XRD) patterns were performed using an X-ray diffraction system (Smartlab9, Japan) with Cu KR radiation (λ=1.5406 Å). The Fourier transform infrared spectroscopy (FTIR, Nicolet 380 FTIR-ATR) and X-ray photoelectron spectrometer (XPS, ESCALAB 250Xi) of samples were used to analyze the chemical composition. The size distribution of oil droplet in the O/W emulsion and filtration was provided by nanoparticle size analyzer (DLS, Malvern Zetasizer Nano ZS90). Optical images of the O/W emulsion before and after separation were obtained from a microscope (Olympus, Japan) by dropping the solution on a wafer. The content of oil in water was monitor by Infrared oil meters (OIL 450).

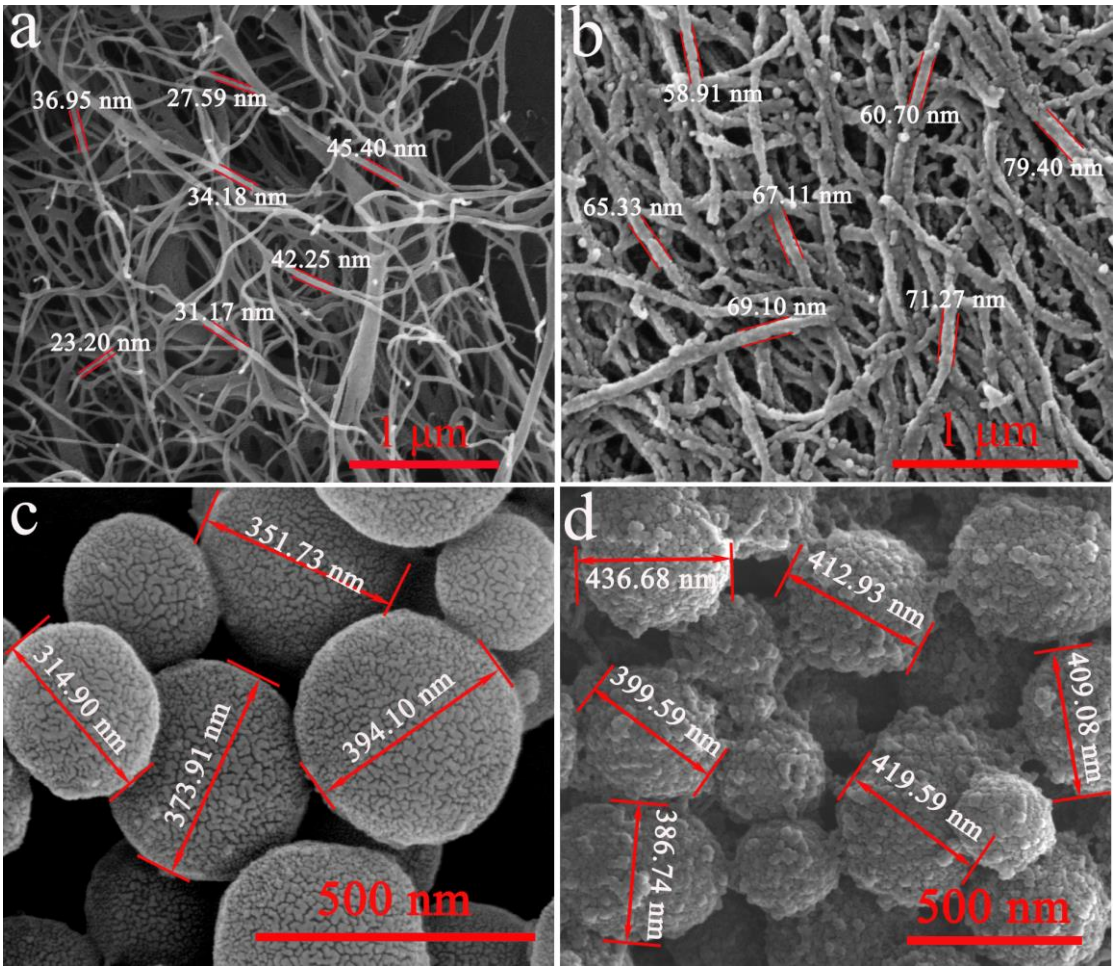

Fig. S2. The SEM images of BC (a), PBC (b), PSM (c) and PPSM (d).

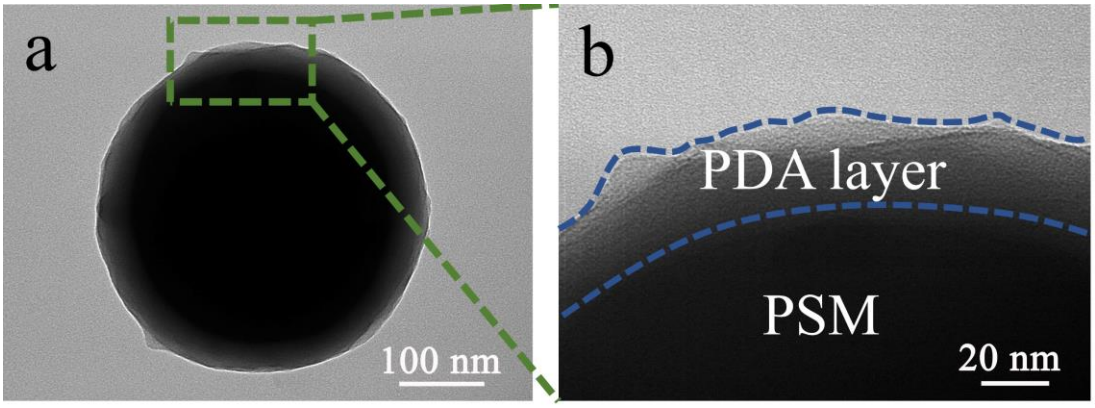

Fig. S3. (a) The TEM image and (b) it responding High-resolution image of PPSM.

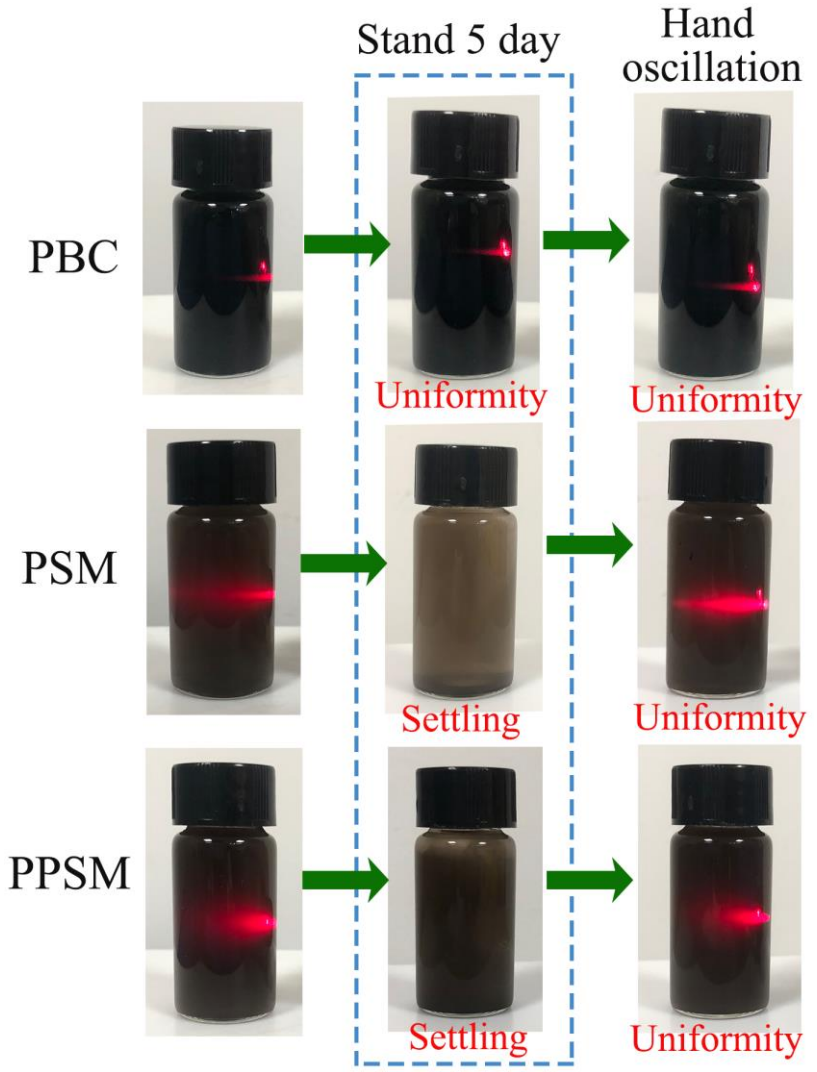

Fig. S4. Dispersion stability of PBC, PSM and PPSM in aqueous solutions.

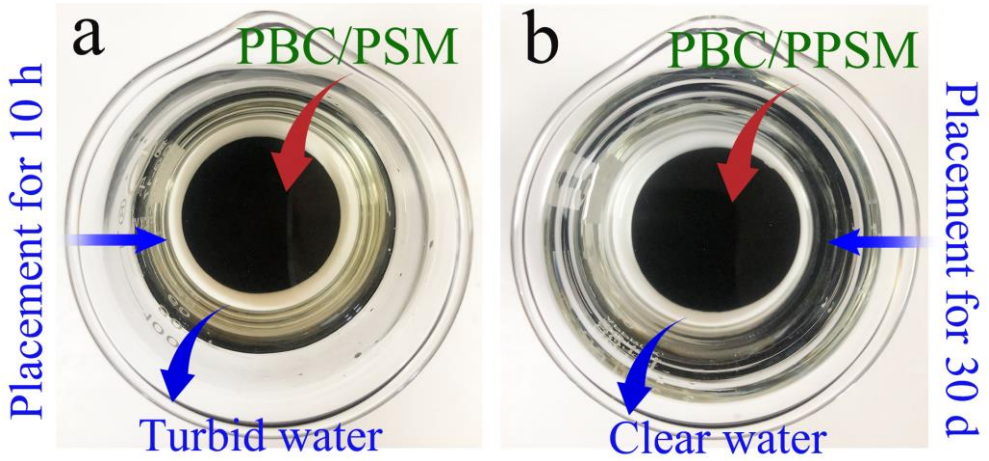

Fig. S5. (a) Optical photograph of PBC/PSM film immersed in water for 10 h. (b) Optical photograph of PBC/PPSM film immersed in water for 30 d.

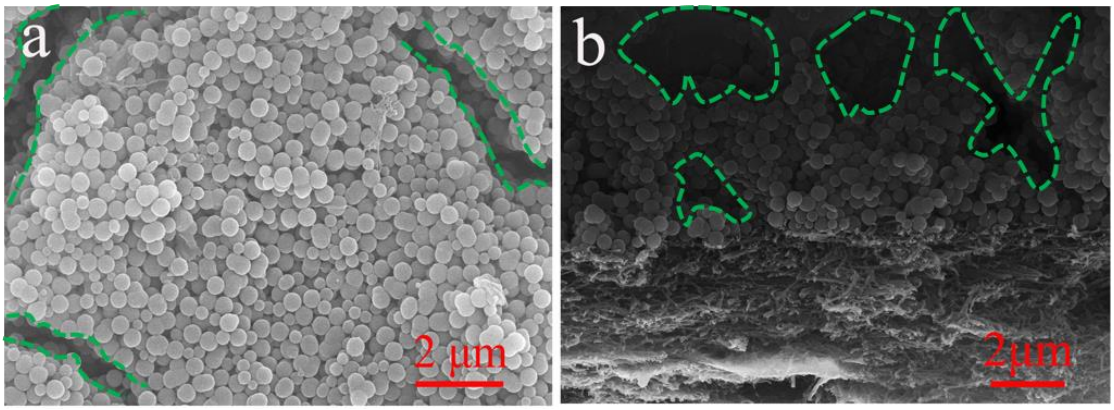

Fig. S6. (a) Surface micromorphology of PBC/PSM composite film. (b) Cross section micromorphology of PBC/PSM composite film.

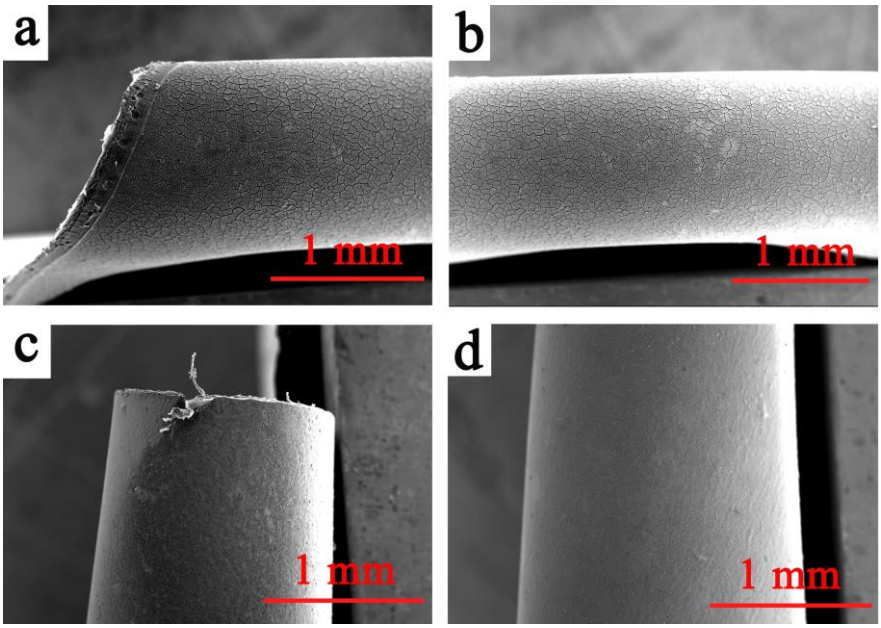

Fig. S7. SEM images of PBC/PSM (a, b) and PBC/PPSM (c, d) composite films in bending condition

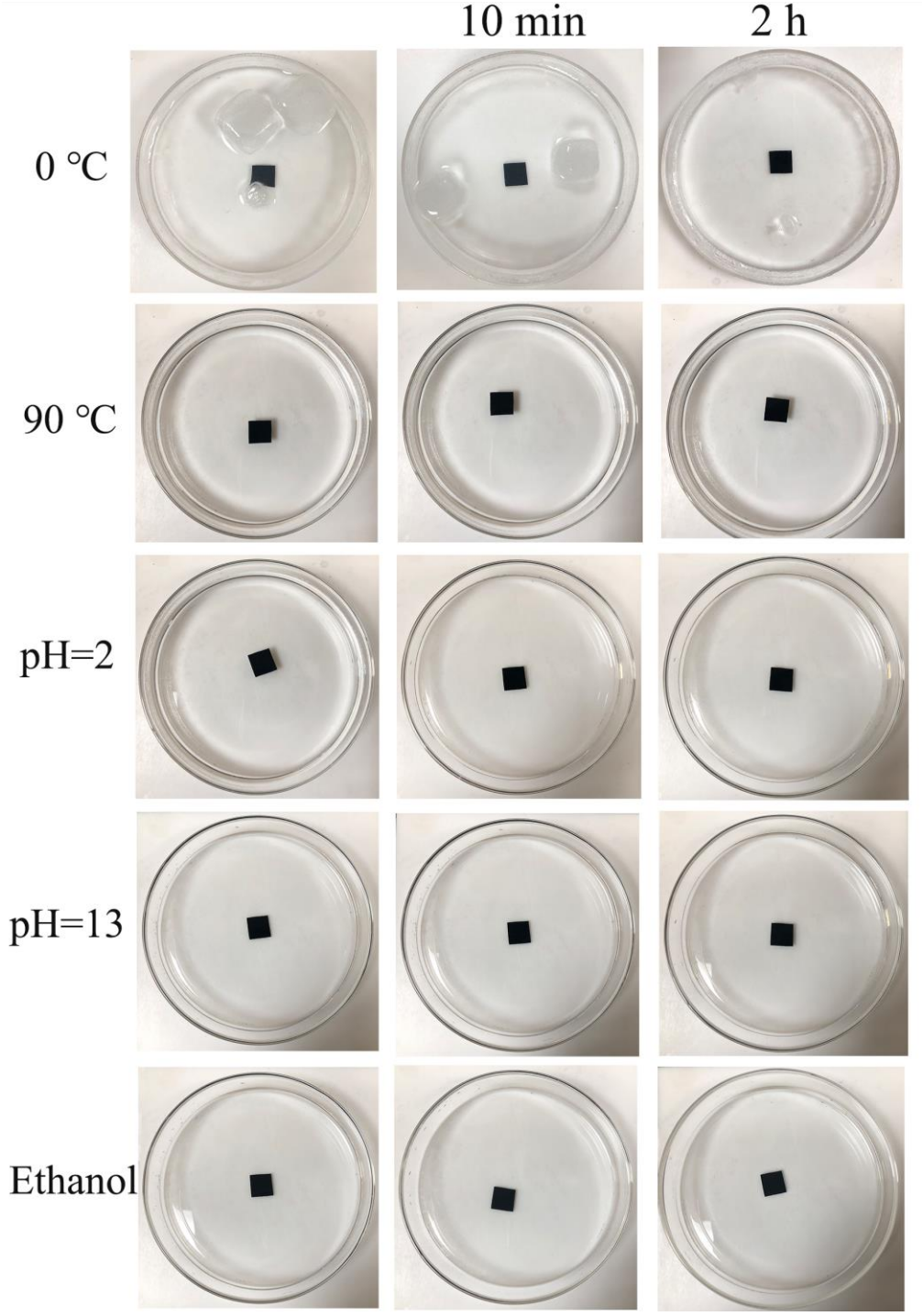

Fig. S8. Morphological stability of PBC/PPSM composite films in different aqueous environments.

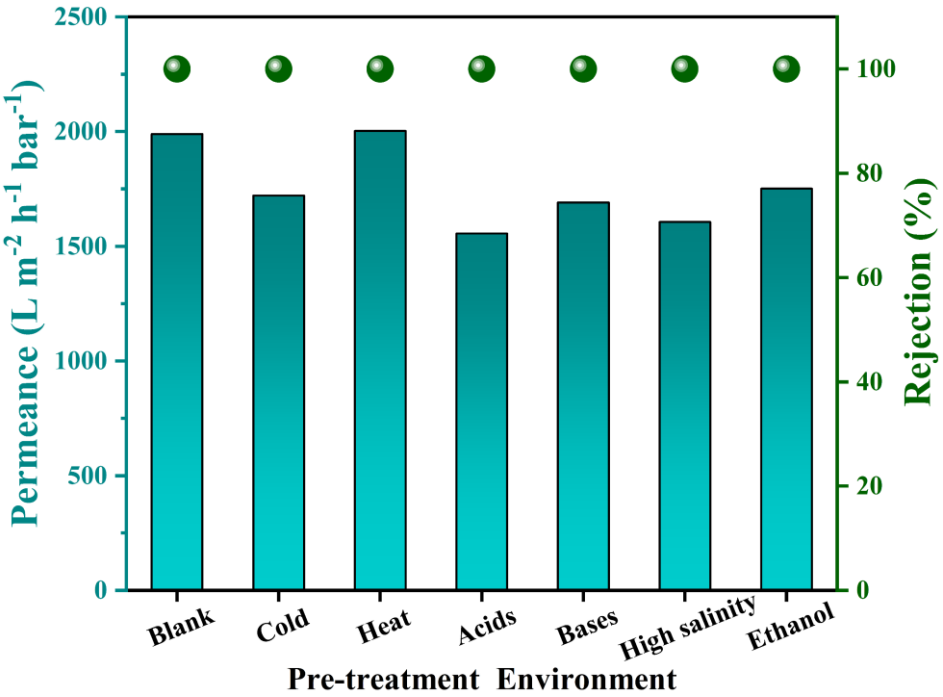

Fig. S9. Separation performance of composite films for RhB after 2 h pretreatment in several complex environment.

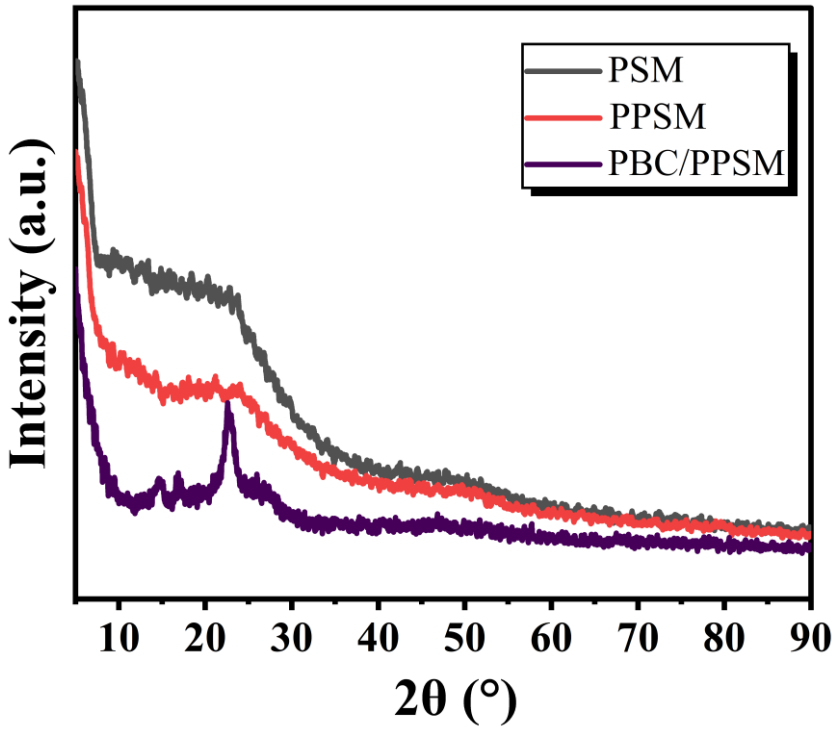

Fig. S10. The XRD spectra of the PSM, PPSM and PBC/PPSM.

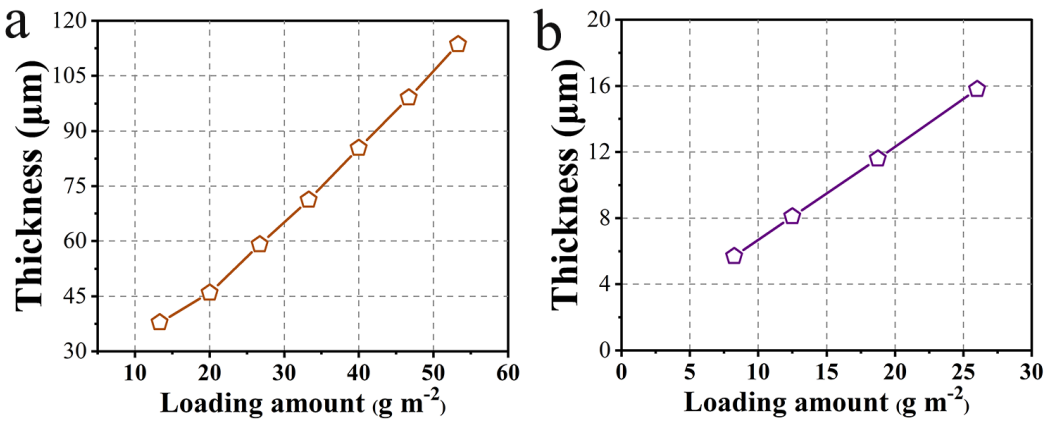

Fig. S11. PBC film thickness with different 1D PBC loading amounts. (b) PPSM layer thickness in PBC/PPSM film with different 0D PPSM loading amounts (PBC loading amounts: 33.3g m^{-2}).

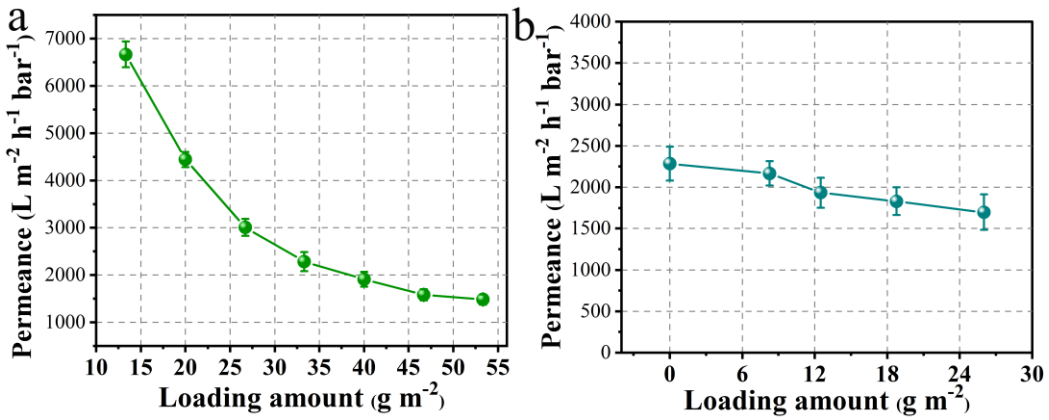

Fig. S12. (a) Pure water permeance of PBC films with different 1D PBC loading amounts. (b) Pure water permeance of PBC/PPSM films with different 0D PPSM loading amounts (PBC loading amounts: 33.3 g m^{-2}).

Pure water permeances were studied to investigate the mass transfer characteristics of water molecules in the fluid channels of the PBC/PPSM structure. The water permeances on PBC/PPSM films obtained with different PBC loadings has significant variations. The effect of film thickness on water permeance is consistent with previous studies[2, 3]. Compared to pure PBC films, the addition of PPSM not only does not result in lower water permeance, but also improves it. This is not only because of the small effect of PPSM on the film thickness, but more importantly, the positive effect of the nanofluidic structure constructed by PPSM nano/microspheres on the flow of water molecules. Water permeance increases near linearly with increasing pressure, which indicates that the nanochannels in the composite film do not shrink, and retain sufficient rigidness and mechanical properties even under an influent pressure of 4 bar.

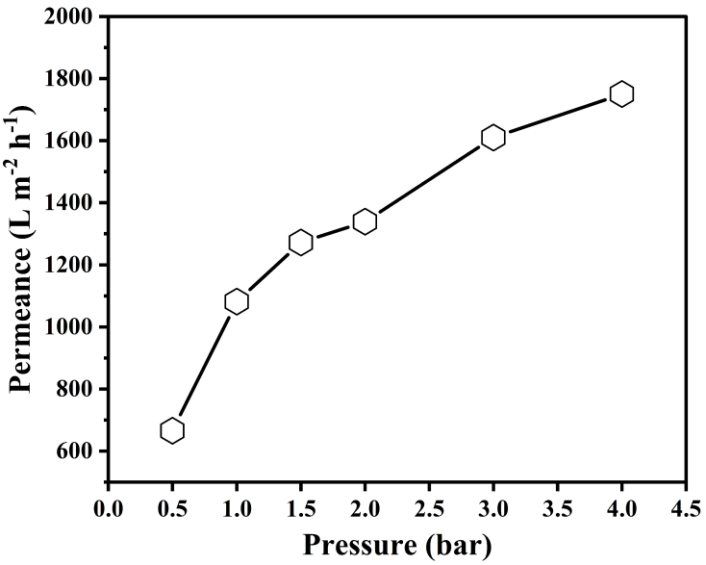

Fig. S13. The water permeance of composite films at different influent pressures.

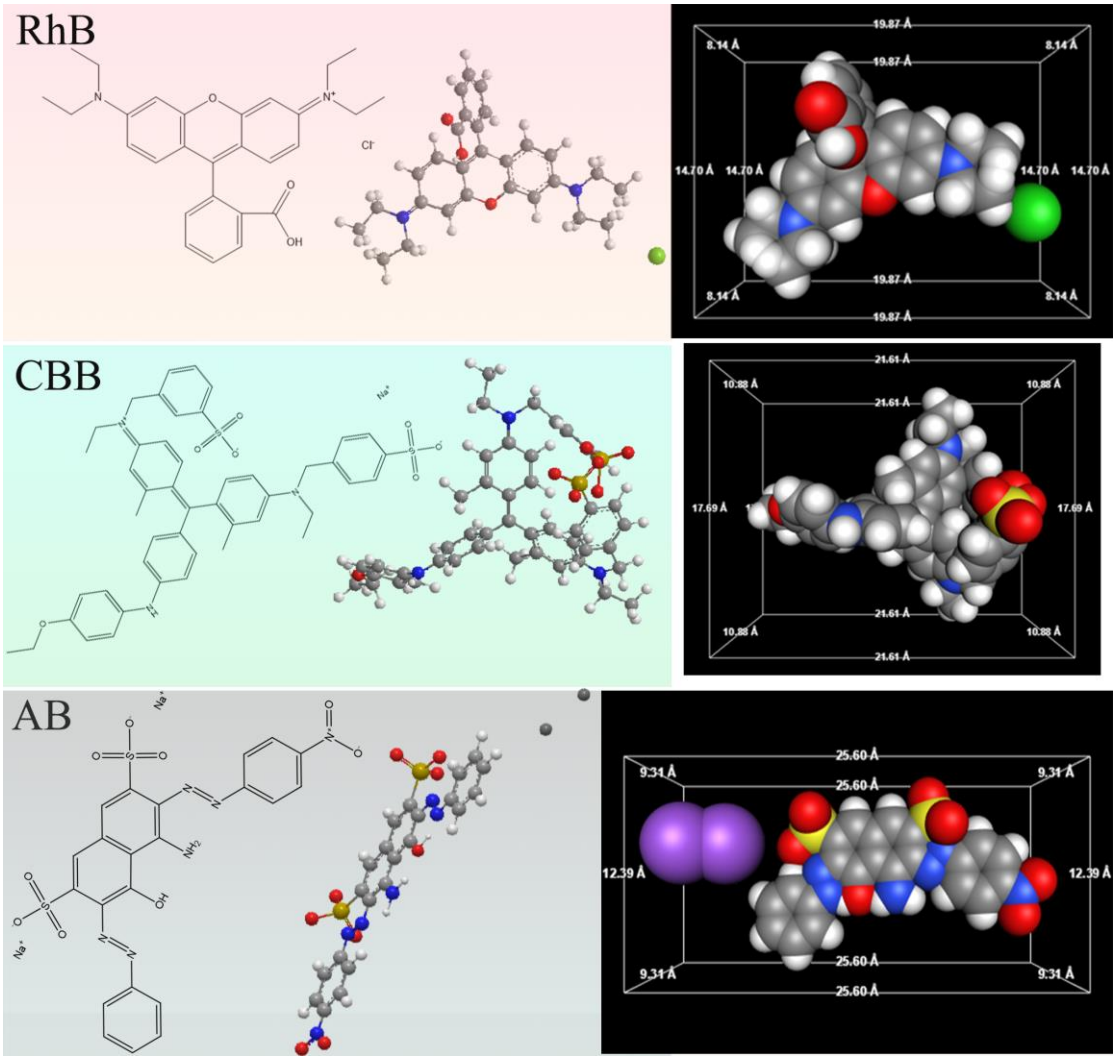

Fig. S14. The molecular formula, molecular structure, and three-dimensional dimensions of the dye molecules (RhB, CBB and BF).

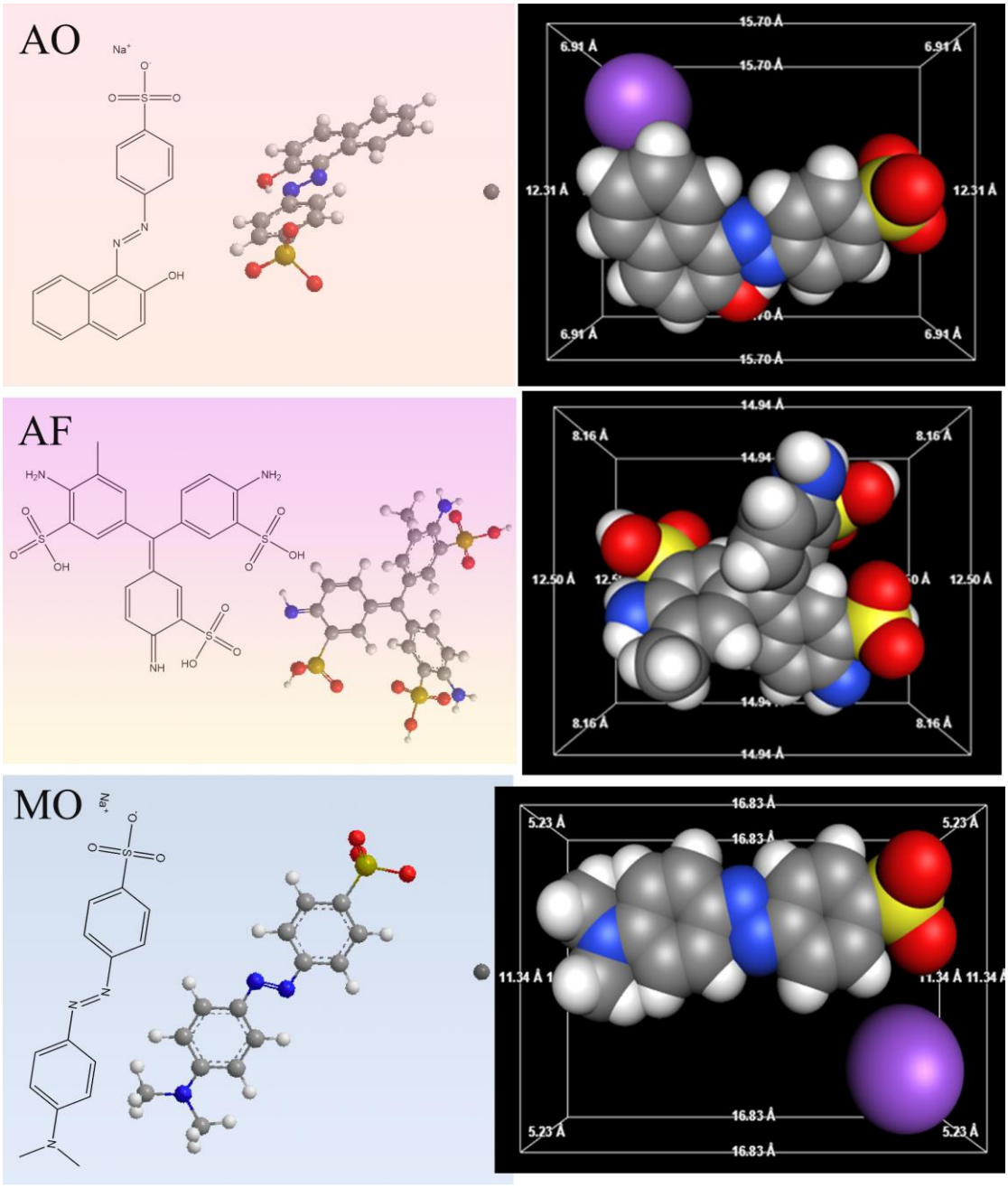

Fig. S15. The molecular formula, molecular structure, and three-dimensional dimensions of the dye molecules (AB, AO and AF).

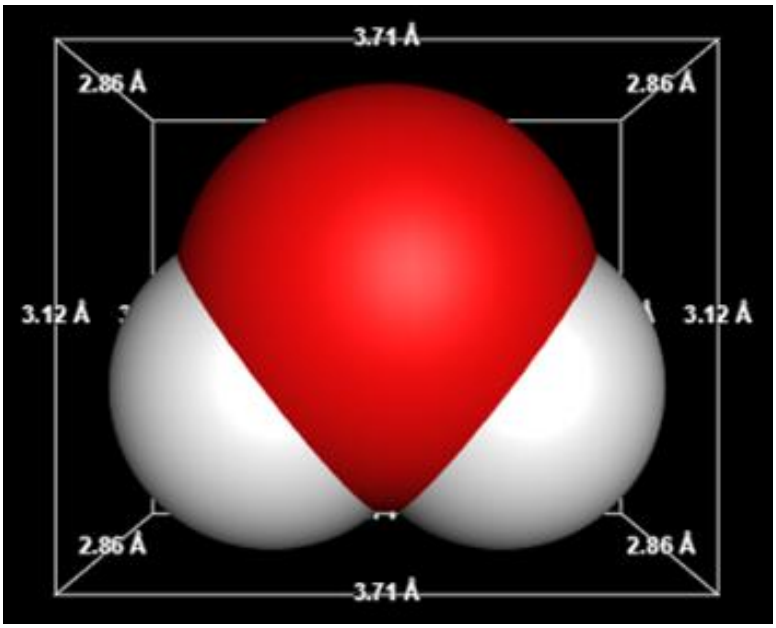

Fig. S16. The three-dimensional dimensions of the water molecules.

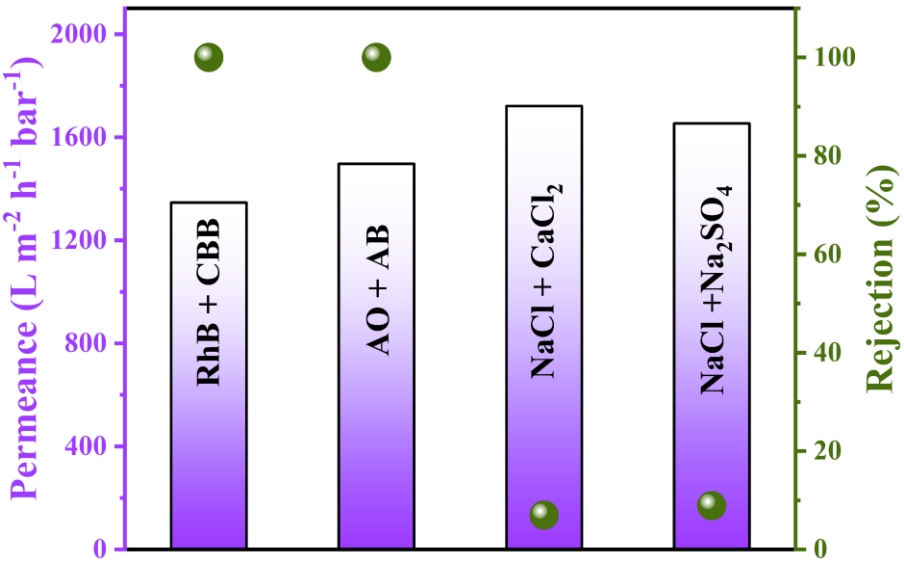

Fig. S17. Separation performance of composite films for different mixed dyes and mixed salt ions.

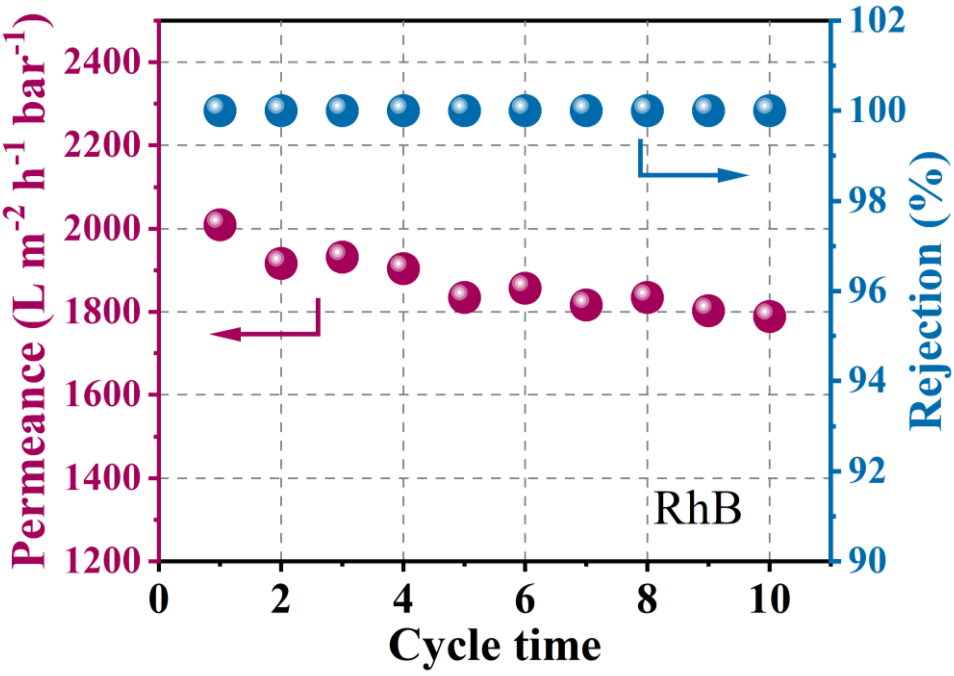

Fig. S18. The permeance and RhB rejections of PBC/PPSM films with 10 periodic operations of dye filtering.

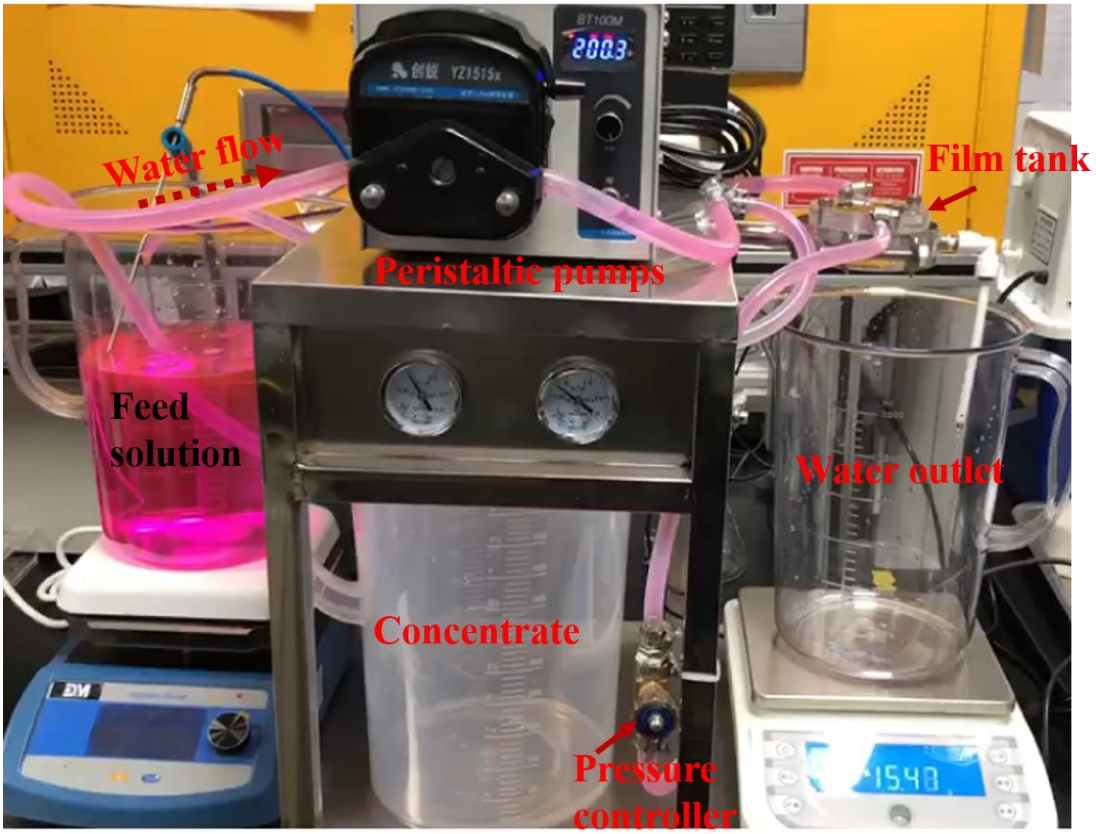

Fig. S19. Physical diagram of cross-flow filtration device.

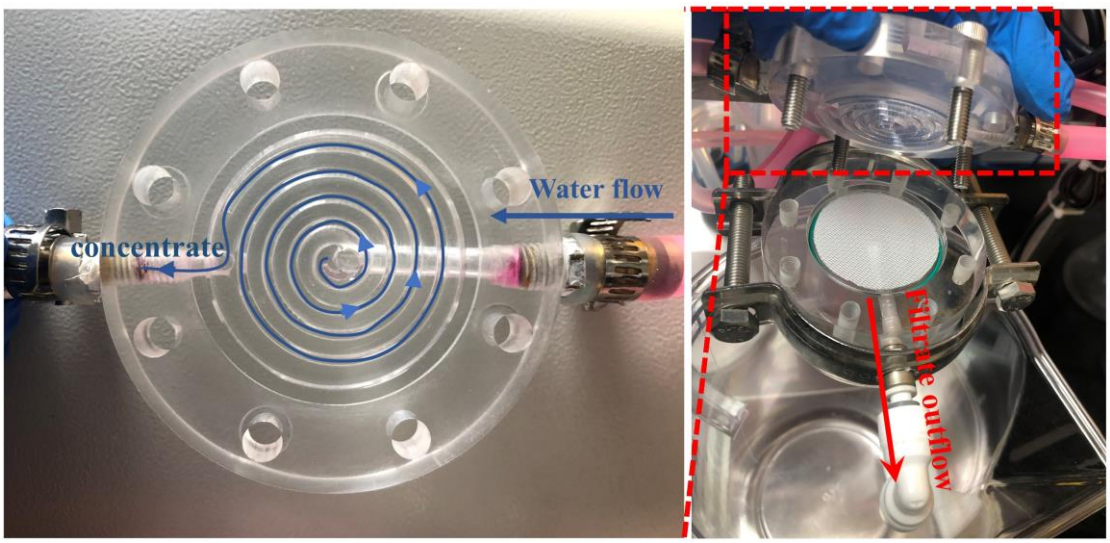

Fig. S20. Internal structure and water flow path of film tank.

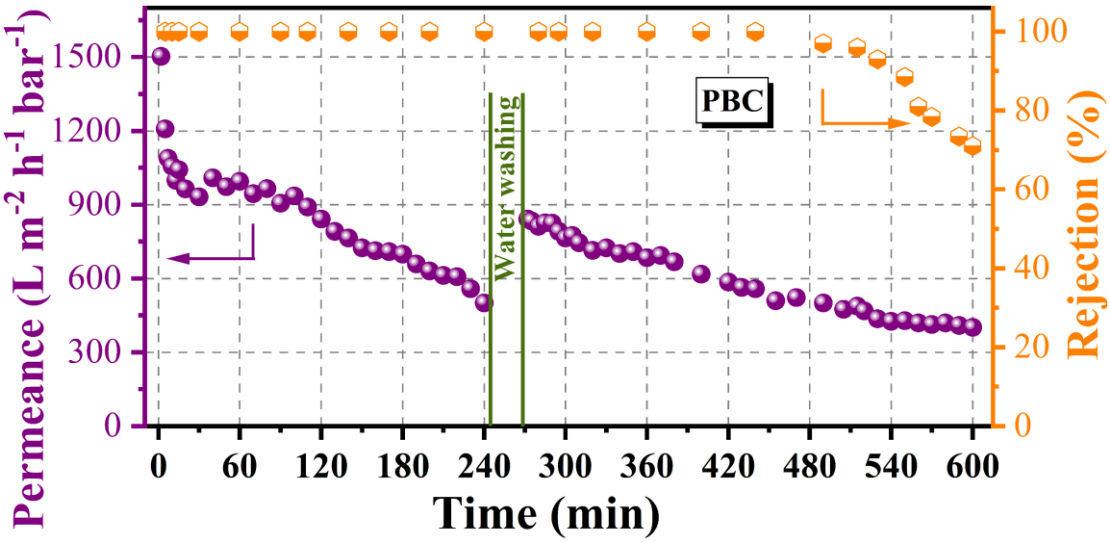

Fig. S21. Separation efficiency of PBC composite film for long time separation of RhB solution under cross-flow filtration (RhB concentration: 5 mg/L).

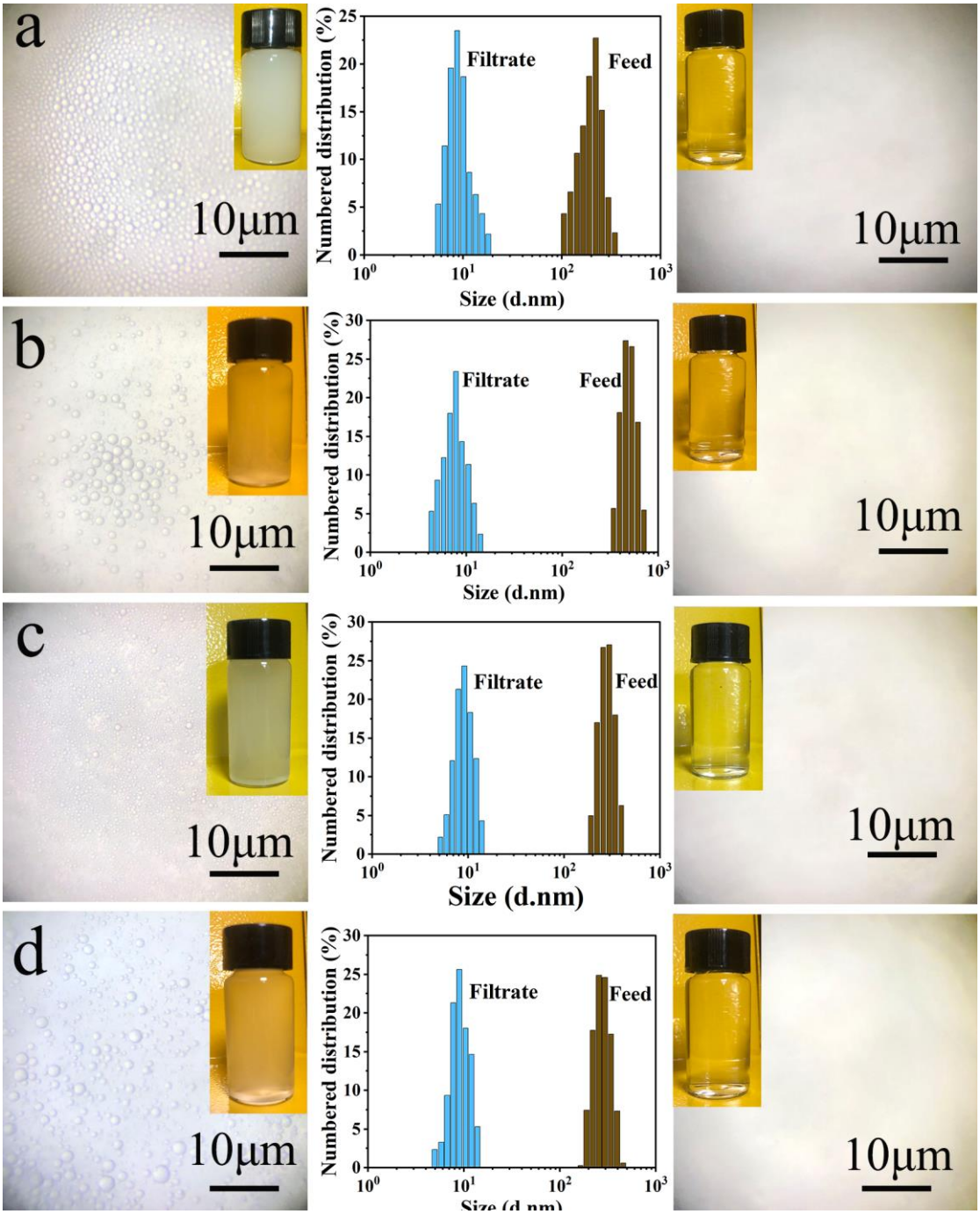

Fig. S22. The microscopic images and nano particle size test results of (a) V/W emulsion, (b) H/W emulsion, (c) L/W emulsion, (d) P/W emulsion before and after separation, respectively.

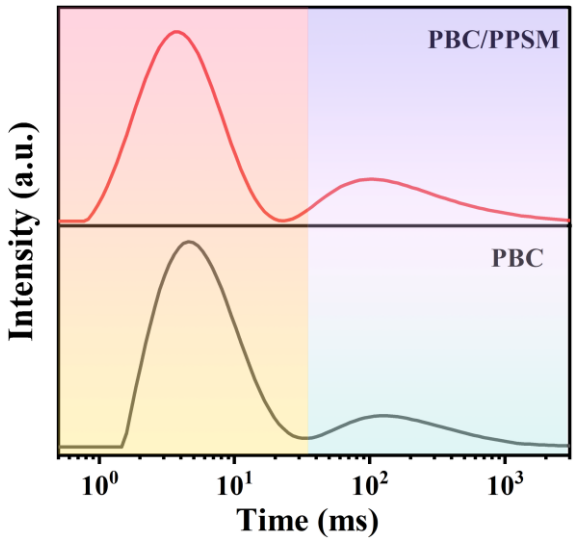

Fig. S23. ^{1}H time-domain LF-NMR spectra of PBC and PBC/PPSM.

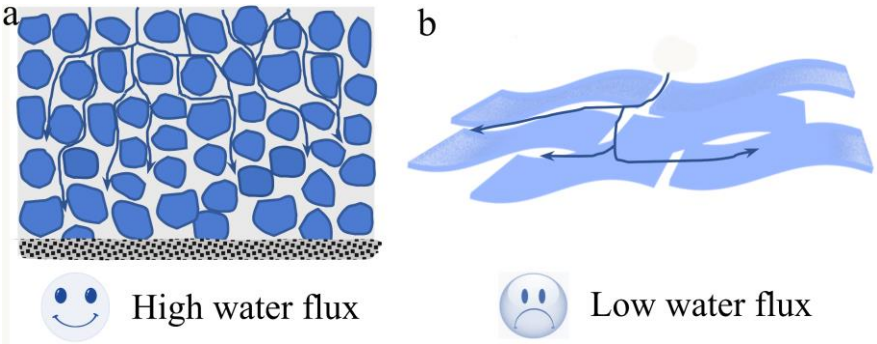

Fig. S24. Inter-particle pores (a) are more conducive to water flow than two-dimensional nanofilm inter-layer channels (b)

Table S1. Comparison of dye rejection performance of various films under dead-end filtration

Films	Dye	Initial concentration (mg/L)	Pressure (bar)	Permeance (L m^{-2} h^{-1} bar^{-1})	Rejection (%)	Ref.
DA-NMG/GA	MB	50	3.5	10.29	99.0	[4]
LNFM	CR	20	2	87.1	99.6	[5]
GO-TA-Ni	CR	50	1	71.7	97	[6]
PGOM	MB	10	1	131.1	99	[7]
PES/β-CD	CR	20	2	30.5	97.4	[8]
ZIF-8/PVDF	RhB	10	1	137	97.5	[9]
GO/APT	RhB	7.5	0.9	14.7	100	[10]
PSf-b-PEG	DR	35	1	63.1	93.1	[11]
Ca/GO-SA3	MB	20	1.2	38.9	99	[12]
NiOH-MEM	DY	20	0.5	99	97.3	[13]
M-7	CR	20	2	40.6	99.6	[14]
PBC/PPSM	**RhB**	**10**	**1**	**1980**	**100**	**This work**

MB: Methylene blue; CR: Congo red; RhB: Rhodamine B; DR: Direct red; DY: Direct yellow.

Table S2. Comparison of the performance of various films in dye/salt separation

Films	Pressure (bar)	Permeance (L m^{-2} h^{-1} bar^{-1})	Dye/R_{dye} (%)	R_{salt} (%)	Ref.
PBC/PPSM	**0.4**	**600**	**RhB: 100**	**NaCl: 3.4 Na_2SO_4: 4.9 $CaCl_2$: 6.1**	**This work**
β-CD/TMC	2	103.9	CR: 100	NaCl: 8.5	[15]
PSF-COOH60%	1	153.8	CR: 95.5	NaCl: 5.6	[16]
PVDF/SMANa	1	251.6	MB: 96.7	$MgCl_2$: 4.5	[17]
PEI/TA/PES	4	40.6	CR: 99.8	NaCl: 6.1 Na_2SO_4: 2.2	[18]
PEI/PDA/PES	2	7.2	MB: 96.5	$MgCl_2$: 19.9	[19]
PEI/CMCNa/PP	3	5.7	CR: 99.8	Na_2SO_4: 19	[20]
ePDA-10	1.5	7.8	CR: 98	NaCl: 1.8 Na_2SO_4: 6	[21]
SiO_2-PSS-PES	4	67.2	RR: 85	NaCl: 17	[22]
CS-MMT-PES	4	17.8	RR: 90	NaCl: 15	[23]
COF/Al_2O_3	5	53.4	AF: 90 CBT: 99	NaCl: 4.5 $MgCl_2$: 5.4	[24]
ZIF-8/PEI-HPAN	1	78	CR: 98.9	NaCl: 4.5	[25]
Sepro NF 6	6	13.7	DR: 99.9	NaCl: 2.5	[26]
ZIF-8@ZNPM	4	192.4	CR: 98	Na_2SO_4: 3.2	[27]
LNMs	4	7.16	CR: 97.47	NaCl: 2.55	[28]
TFN-0.2	6	56	DR: 99.8	NaCl: 8.8	[29]
DAT/TMC TFC	2	95.1	CR: 99.1	NaCl: 5.8	[30]
GO/NH_2-Fe_3O_4	5	78	CR: 94	NaCl: 15	[31]
SMA-PEI/PES	2	23	CR: 99.4	NaCl: 2.5	[32]
AM-PEI/HPAN	4	42.9	MB: 99.2 CR: 98.6	NaCl: 4.4 $MgCl_2$: 15.6	[33]
CNT/GO	1	26.3	CR: 98.7 MB: 94.1	NaCl: 3.1 Na_2SO_4: 6.3	[34]

RR: Reactive Red; CBT: Chrome black T; DR: Direct red.

References

1. X. Li, X. Chu and D. C. Sheng, *Int. J. Numer. Methods Eng.*, 2007, **72**, 858-882.
2. S. Ling, K. Jin, D. L. Kaplan and M. J. Buehler, *Nano Lett.*, 2016, **16**, 3795-3800.
3. S. Ling, Z. Qin, W. Huang, S. Cao, D. L. Kaplan and M. J. Buehler, *Sci. Adv.*, 2017, **3**.
4. Y. Chen and C. He, *Desalination*, 2017, **413**, 29-39.
5. P. Jin, J. Zhu, S. Yuan, G. Zhang, A. Volodine, M. Tian, J. Wang, P. Luis and B. Van der Bruggen, *Chem. Eng. J.*, 2021, **406**.
6. X. Kang, Y. Cheng, Y. Wen, J. Qi and X. Li, *J. Hazard. Mater.*, 2020, **400**, 123121.
7. J.-J. Lu, Y.-H. Gu, Y. Chen, X. Yan, Y.-J. Guo and W.-Z. Lang, *Sep. Purif. Technol.*, 2019, **210**, 737-745.
8. L. Zhang, H. Guan, N. Zhang, B. Jiang, Y. Sun and N. Yang, *Sep. Purif. Technol.*, 2019, **218**, 8-19.
9. Y. Guo, X. Wang, P. Hu and X. Peng, *Appl. Mater. Today*, 2016, **5**, 103-110.
10. C.-Y. Wang, W.-J. Zeng, T.-T. Jiang, X. Chen and X.-L. Zhang, *Sep. Purif. Technol.*, 2019, **214**, 21-30.
11. C. Xu, C. Wang, X. He, M. Lyu, S. Wang and L. Wang, *J. Hazard. Mater.*, 2017, **325**, 214-222.
12. J. Yu, Y. Wang, Y. He, Y. Gao, R. Hou, J. Ma, L. Zhang, X. Guo and L. Chen, *Sep. Purif. Technol.*, 2021, **276**.
13. Y. Qu, Q. G. Zhang, F. Soyekwo, R. S. Gao, R. X. Lv, C. X. Lin, M. M. Chen, A. M. Zhu and Q. L. Liu, *Nanoscale*, 2016, **8**, 18428-18435.
14. J. Li, S. Yuan, J. Zhu and B. Van der Bruggen, *Chem. Eng. J.*, 2019, **373**, 275-284.
15. L. Liu, L. Yu, B. Borjigin, Q. Liu, C. Zhao and D. Hou, *Appl. Surf. Sci.*, 2021, **539**, 148284.
16. Z. Liu, L. Wang, Z. Mi, S. Jin, D. Wang, X. Zhao, H. Zhou and C. Chen, *Appl. Surf. Sci.*, 2019, **490**, 7-17.
17. D. Kang, H. Shao, G. Chen, X. Dong and S. Qin, *J. Membr. Sci.*, 2021, **621**, 118951.
18. Q. Li, Z. Liao, X. Fang, D. Wang, J. Xie, X. Sun, L. Wang and J. Li, *J. Membr. Sci.*, 2019, **584**, 324-332.
19. R. Zhang, Y. Su, X. Zhao, Y. Li, J. Zhao and Z. Jiang, *J. Membr. Sci.*, 2014, **470**, 9-17.
20. Q. Chen, P. Yu, W. Huang, S. Yu, M. Liu and C. Gao, *J. Membr. Sci.*, 2015, **492**, 312-321.
21. J. Wang, X. Pei, G. Liu, Q. Han, S. Yang and F. Liu, *J. Membr. Sci.*, 2019, **586**, 170-176.
22. L. Xing, N. Guo, Y. Zhang, H. Zhang and J. Liu, *Sep. Purif. Technol.*, 2015, **146**, 50-59.
23. J. Zhu, M. Tian, Y. Zhang, H. Zhang and J. Liu, *Chem. Eng. J.*, 2015, **265**, 184-193.
24. H. Fan, J. Gu, H. Meng, A. Knebel and J. Caro, *Angew. Chem. Int. Ed.*, 2018, **57**, 4083-4087.
25. L. Yang, Z. Wang and J. Zhang, *J. Mater. Chem. A*, 2017, **5**, 15342-15355.

26. J. Lin, W. Ye, H. Zeng, H. Yang, J. Shen, S. Darvishmanesh, P. Luis, A. Sotto and B. Van der Bruggen, *J. Membr. Sci.*, 2015, **477**, 183-193.
27. Y.-L. Ji, B.-X. Gu, S.-J. Xie, M.-J. Yin, W.-J. Qian, Q. Zhao, W.-S. Hung, K.-R. Lee, Y. Zhou, Q.-F. An and C.-J. Gao, *Adv. Mater.*, 2021, **33**.
28. Q. Li, Z. Liao, X. Fang, J. Xie, L. Ni, D. Wang, J. Qi, X. Sun, L. Wang and J. Li, *Desalination*, 2020, **479**.
29. Y. Song, Y. Sun, N. Zhang, C. Li, M. Hou, K. Chen and T. Li, *Sep. Purif. Technol.*, 2021, **271**.
30. X. Feng, D. Liu, H. Ye, D. Peng, J. Wang, S. Han and Y. Zhang, *Sep. Purif. Technol.*, 2022, **278**.
31. L. Dong, M. Li, S. Zhang, X. Si, Y. Bai and C. Zhang, *Desalination*, 2020, **476**.
32. J. Jin, X. Du, J. Yu, S. Qin, M. He, K. Zhang and G. Chen, *J. Membr. Sci.*, 2020, **611**.
33. L. Zhang, L. Xu, H. Yu, P. Yao, M. Zhang, F. Guo and L. Yu, *J. Membr. Sci.*, 2022, **641**.
34. L. Huang, Z. Li, Y. Luo, N. Zhang, W. Qi, E. Jiang, J. Bao, X. Zhang, W. Zheng, B. An and G. He, *Sep. Purif. Technol.*, 2021, **256**.